A New Polymorph of ZrW_2O_8 Prepared Using Nonhydrolytic Sol−Gel Chemistry

Angus P. Wilkinson,* Cora Lind, and Sidhartha Pattanaik

School of Chemistry and Biochemistry, Georgia Institute of Technology, Atlanta, Georgia 30332-0400

Received July 17, 1998. Revised Manuscript Received October 15, 1998

A new polymorph of ZrW_2O_8, structurally related to trigonal $ZrMo_2O_8$, has been prepared at low temperatures using nonhydrolytic sol−gel chemistry. Its identity was established by powder X-ray diffraction, energy dispersive X-ray analysis, and extended X-ray absorption fine structure (EXAFS). This material is denser than the previously reported cubic and orthorhombic forms of ZrW_2O_8 and decomposes into the binary oxides on prolonged heating at 700 °C. An EXAFS investigation of the crystallization of "ZrW_2O_8" gels, prepared by nonhydrolytic methods, suggests that the coordination environments of the cations in the heat-treated gels evolve toward those found in the new form of ZrW_2O_8 prior to the crystallization of this product.

Introduction

Cubic zirconium tungstate (ZrW_2O_8) was first prepared almost 40 years ago.[1] It is the only ternary phase appearing in the atmospheric pressure ZrO_2−WO_3 pseudobinary phase diagram.[2,3] While the material has been known to exhibit negative thermal expansion for some time,[4] it has recently received considerable attention because it undergoes isotropic negative thermal expansion over a very large temperature range: 0.3−1050 K.[5−11] While there are often similarities between the structural chemistry of molybdenum and tungsten, the compound $ZrMo_2O_8$ was until 1998 only known to occur in trigonal and monoclinic forms.[12−15] Recently, we have reported the preparation of a new metastable cubic $ZrMo_2O_8$ with a structure closely related to that of cubic ZrW_2O_8.[16]

Cubic ZrW_2O_8 is thermodynamically stable in the temperature range 1105−1257 °C[2] and metastable with respect to the component binary oxides below ∼780 °C. The preparation of materials under conditions where they are metastable is very demanding of the synthetic chemistry employed. In the case of ZrW_2O_8, a preparation below ∼780 °C requires that (i) the precursor material is compositionally homogeneous on a short length scale and (ii) the crystallization to give ZrW_2O_8 is significantly faster than the long-range metal ion diffusion that would give rise to the thermodynamically favored phase separation.

There are several possible routes to the low-temperature synthesis of a material such as ZrW_2O_8. However, we chose to explore the use of nonhydrolytic sol−gel chemistry[17,18] as it has recently been promoted as a good method for the preparation of compositionally homogeneous precursors suitable for the synthesis of metastable phases.[17,19] The use of nonhydrolytic sol−gel methods for the preparation of metal oxides, in particular the reactions of alkoxides with metal halides, or ethers with metal halides, to produce M−O−M links and an alkyl halide, has only recently received considerable attention even though the method is relatively old. For example, in the 1950s syntheses for silica and boron phosphate[20] using this approach were reported. Recently, there has been work on SiO_2,[21] TiO_2,[22−25] ZrO_2,[23] WO_3,[23] Al_2TiO_5,[19,26] $Al_6Si_2O_{13}$,[27] Al_2O_3,[22,28] Nb_2O_5,[23]

(1) Graham, J.; Wadsley, A. D.; Weymouth, J. H.; Williams, L. S. *J. Am. Ceram. Soc.* **1959**, *42*, 570.
(2) Chang, L. L. Y.; Scroger, M. G.; Phillips, B. *J. Am. Ceram. Soc.* **1967**, *50*, 211−215.
(3) Martinek, C. A.; Hummel, F. A. *J. Am. Ceram. Soc.* **1970**, *53*, 159−161.
(4) Martinek, C.; Hummel, F. A. *J. Am. Ceram. Soc.* **1968**, *51*, 227−228.
(5) Evans, J. S. O.; Mary, T. A.; Vogt, T.; Subramanian, M. A.; Sleight, A. W. *Chem. Mater.* **1996**, *8*, 2809−2823.
(6) Evans, J. S. O.; Hu, Z.; Jorgensen, J. D.; Argyriou, D. N.; Short, S.; Sleight, A. W. *Science* **1997**, *275*, 61−65.
(7) Mary, T. A.; Evans, J. S. O.; Vogt, T.; Sleight, A. W. *Science* **1996**, *272*, 90−92.
(8) Perottoni, C. A.; de Jornada, J. A. H. *Science* **1998**, *280*, 886−889.
(9) Pryde, A. K. A.; Hammonds, K. D.; Dove, M. T.; Heine, V.; Gale, J. D.; Warren, M. C. *J. Phys. Condens. Matter* **1996**, *8*, 10973−10982.
(10) Pryde, A. K. A.; Hammonds, K. D.; Dove, M. T.; Heine, V.; Gale, J. D.; Warren, M. C. *Phase Transitions* **1997**, *61*, 141−153.
(11) Seo, D.-K.; Whangbo, M.-H. *J. Solid State Chem.* **1997**, *129*, 160−163.
(12) Auray, M.; Quarton, M.; Tarte, P. *Acta Crystallogr.* **1986**, *C42*, 257−259.
(13) Auray, M.; Quarton, M.; Tarte, P. *Powder Diffract.* **1987**, *2*, 36−38.
(14) Auray, M.; Quarton, M. *Powder Diffract.* **1989**, *4*, 29−30.
(15) Serezhkin, V. N.; Efremov, V. A.; Trunov, V. K. *Russ. J. Inorg. Chem.* **1987**, *32*, 1566−1570.
(16) Lind, C.; Wilkinson, A. P.; Hu, Z.; Short, S.; Jorgensen, J. D. *Chem. Mater.* **1998**, *10*, 2335−2337.
(17) Vioux, A. *Chem. Mater.* **1997**, *9*, 2292−2299.
(18) Vioux, A.; Leclercq, D. *Heterog. Chem. Rev.* **1996**, *3*, 65−73.
(19) Andrianainarivelo, M.; Corriu, R. J. P.; Leclercq, D.; Mutin, P. H.; Vioux, A. *Chem. Mater.* **1997**, *9*, 1098−1102.
(20) Gerrard, W.; Griffey, P. F. *Chem. Ind. Jan. 10th* **1959**, 55.
(21) Corriu, R. J. P.; Leclercq, D.; Lefevre, P.; Mutin, P. H.; Vioux, A. *J. Non-Cryst. Solids* **1992**, *146*, 301−303.
(22) Corriu, R. J. P.; Leclercq, D.; Lefevre, P.; Mutin, P. H.; Vioux, A. *J. Mater. Chem.* **1992**, *2*, 673−674.
(23) Arnal, P.; Corriu, R. J. P.; Leclercq, D.; Mutin, P. H.; Vioux, A. *Mater. Res. Soc. Symp. Proc.* **1994**, *346*, 339−344.
(24) Arnal, P.; Corriu, R. J. P.; Leclercq, D.; Mutin, P. H.; Vioux, A. *J. Mater. Chem.* **1996**, *6*, 1925−1932.
(25) Arnal, P.; Corriu, J. P.; Leclerq, D.; Mutin, P. H.; Vioux, A. *Chem. Mater.* **1997**, *9*, 694−698.

10.1021/cm9805065 CCC: $18.00
Published on Web 12/23/1998

V_2O_5,[23] Fe_2O_3,[23] MoO_3,[23] SiO_2-ZrO_2,[29] SiO_2-TiO_2,[29,30] $SiO_2-Al_2O_3$,[30] $Al_2O_3-TiO_2$,[30] and $ZrTiO_4$.[26,31]

Our exploration of nonhydrolytic sol−gel chemistry as a route to the known cubic ZrW_2O_8 led us to the accidental low-temperature preparation of a previously unknown polymorph of this tungstate. This paper reports the crystallization behavior of our "ZrW_2O_8" gels and results from extended X-ray absorption fine structure (EXAFS) studies of the local structure in the starting gels, heat-treated glasses, and crystalline materials for the systems WO_3, ZrO_2, and ZrW_2O_8.

Experimental Section

Syntheses. All steps in the syntheses prior to breaking open the reaction tubes were carried out under an argon atmosphere with dry compounds and solvents. The metal-containing starting materials were purchased from STREM Chemicals, the diisopropyl ether from Aldrich, and the solvents from J. T. Baker. The following detailed procedures are for the samples used in the EXAFS studies. Several variations on the procedure reported for ZrW_2O_8 were tried as part of the crystallization studies.

ZrW_2O_8 via Nonhydrolytic Sol−Gel Processing. First, 2.72 g of WCl_6 (6.8 mmol) were suspended in 10 mL of $CHCl_3$ contained in a glass tube. Then 1.32 g of $Zr(O^iPr)_4 \cdot {}^iPrOH$ (3.4 mmol) were dissolved in a mixture of 8 mL of THF and 2 mL of $^iPr_2O$ (14.2 mmol). The dark brown tungsten-containing suspension was cooled in an ice bath and the zirconium solution was added slowly by syringe while stirring. The ice bath was removed and the mixture stirred for approximately 60 min at room temperature. During this time, the liquid turned midnight blue. The tube was cooled in liquid nitrogen, evacuated, and sealed. It was heated to 110 °C for 7 days. After this time, it contained a dark blue precipitate in a greenish liquid. The tube was broken, the precipitate was suspended in ∼100 mL of $CHCl_3$, and separated by centrifuge. The blue powder, which was dried under vacuum at room temperature, is subsequently called the ZrW_2O_8 raw gel. Three further samples were prepared from the raw gel using the following heat treatments: All samples were heated first to 500 °C for 2 h (heating rate: 5 °/min) and then to 600 °C for another hour (dried gel, carbon free, 30% weight loss). The trigonal material was obtained by heating the dried gel to 740 °C for 30 min in a preheated furnace. The cubic material was prepared by heating to 1200 °C for 15 min in a preheated furnace.

WO_3 via Nonhydrolytic Sol−Gel Processing. 5.13 g of WCl_6 (12.9 mmol) were suspended in 20 mL of $CHCl_3$ in a glass tube. The dark brown suspension was cooled in an ice bath and 5.5 mL of $^iPr_2O$ (38.7 mmol) were added slowly by syringe while stirring. The ice was removed and the mixture was stirred for approximately 90 min at room temperature. During this time, the liquid turned midnight blue. The tube was cooled in liquid nitrogen, evacuated, and sealed. It was heated to 110 °C for 7 days. After this time, it contained a dark blue precipitate in a blue liquid. The tube was broken, the precipitate was suspended in ∼100 mL of $CHCl_3$ and separated by centrifugation. The blue powder was dried under vacuum at room temperature and is subsequently referred to as the raw gel. A dried gel was prepared by heating the raw gel to 350 °C at 5°/min and holding for 1.5 h (9% weight loss relative to the raw gel); a crystalline monoclinic material was obtained on heating to 600 °C for 4 h (12% weight loss relative to the raw gel).

ZrO_2 via Nonhydrolytic Sol−Gel Processing. 5.67 g of $ZrCl_4$ (24 mmol) were suspended in 7 mL of $CHCl_3$ in a glass tube. The opaque mixture was cooled in an ice bath and 14 mL of $^iPr_2O$ (99 mmol) was added slowly by syringe while stirring, giving rise to a purple color. The ice was removed and the mixture was stirred for approximately 30 min at room temperature. During this time, gelation started. The tube was cooled in liquid nitrogen, evacuated, and sealed. It was heated to 110 °C for 7 days. After this time, it contained a white gel in a clear colorless liquid. The tube was broken and the precipitate was suspended in ∼100 mL of $CHCl_3$ and separated by centrifugation. The white powder was dried under vacuum at room temperature and is subsequently referred to as the raw gel. A dried gel was prepared by heating to 200 °C at 5°/min and holding for 2 h (27% weight loss); a crystalline material (mostly tetragonal/cubic, small amount of monoclinic zirconia) was obtained by heating to 600 °C for 4 h (35% weight loss relative to the raw gel).

Powder X-ray Diffraction. Powder X-ray diffraction patterns were recorded for all of the products using a Scintag X1 diffractometer. This instrument was equipped with a Cu Kα radiation source and a Scintag Peltier cooled solid-state detector. For all of the reported data sets, a scan rate of 2.5°/min and a step size of 0.02° were employed along with a 251 mm diffractometer radius, 2/1 mm slits on the tube side, and 0.5/0.3 mm slits on the detector side.

EDX Measurements. The composition of the phase formed by heating the ZrW_2O_8 gel to 740 °C was confirmed by energy dispersive X-ray (EDX) analysis using a Hitachi scanning electron microscope equipped with a Kevex energy-dispersive X-ray detector. Cubic ZrW_2O_8 was used as a reference material for this analysis.

Density Measurements. The density of the "trigonal" ZrW_2O_8 powder was measured pyconometrically; 300−500 mg of powder were used along with a 1 mL volumetric flask and chloroform as the liquid for immersion. Gas bubbles were eliminated from the sample using an ultrasound bath. The measurement was repeated four times and an average value computed.

EXAFS Data Collection. EXAFS data for the samples were collected using beam line 2-3 at the Stanford Synchrotron Radiation Laboratory. All measurements were made at room temperature in transmission using a three-ion chamber arrangement with the sample between the first and second detector and a reference metal foil between the second and third detector. The samples were diluted and ground with boron nitride so that the maximum value of μt (μ = absorption coefficiently, t = sample thickness) was ∼2. A Si(111) double crystal monochromator was used for all of the measurements along with slits defining a beam size of 15 × 2 mm at the sample position. The measurements at the W L_{III}- and Zr K-edges were performed using 40% and 20% monochromator detuning, respectively (quoted values are for the end of the scan range). The energy resolution was estimated to be ∼6 and 17 eV at the W L_{III}- and Zr K-edges, respectively. A summary of the data collected and the sample naming scheme is presented in Table 1.

EXAFS Data Analysis. The EXAFS data analyses were performed using the program package EXAFSPAK.[32] Phase and amplitude functions were calculated using the program FEFF6.[33]

The zirconium K-edge EXAFS data were compared with models derived from the crystal structures of monoclinic zirconia,[34] tetragonal zirconia,[34] cubic ZrW_2O_8,[7] and trigonal $ZrMo_2O_8$.[12] As the local environment of zirconium in monoclinic zirconia is irregular (seven distinct Zr−O distances between 2.04 and 2.27 Å) the Zr−O distances were not varied during

(26) Andrianainarivelo, M.; Corriu, R. J. P.; Leclercq, D.; Mutin, P. H.; Vioux, A. *J. Sol−Gel Sci. Technol.* **1997**, *8*, 89−93.
(27) Acosta, S.; Corriu, R. J. P.; Leclercq, D.; Mutin, P. H.; Vioux, A. *Mater. Res. Soc. Symp. Proc.* **1994**, *346*, 345−350.
(28) Acosta, S.; Corriu, R. J. P.; Leclercq, D.; Lefevre, P.; Mutin, P. H.; Vioux, A. *J. Non-Cryst. Solids* **1994**, *170*, 234−242.
(29) Andrianainarivelo, M.; Corriu, R.; Leclercq, D.; Mutin, P. H.; Vioux, A. *J. Mater. Chem.* **1996**, *6*, 1665−1671.
(30) Corriu, R.; Leclercq, D.; Lefevre, P.; Mutin, p. H.; Vioux, A. *Chem. Mater.* **1992**, *4*, 961−963.
(31) Andrianainarivelo, M.; Corriu, R. J. P.; Leclercq, D.; Mutin, P. H.; Vioux, A. *J. Mater. Chem.* **1997**, *7*, 279−284.
(32) George, G. N.; Pickering, I. J. *EXAFSPAK A Suite of Programs for Analysis of X-ray Absorption Spectra*, 1995.
(33) Zabinsky, S. I.; Rehr, J. J.; Ankubinov, A.; Albers, R. C.; Eller, M. J. *Phys. Rev. B* **1995**, *52*, 2995.
(34) Bondars, B.; Heidemane, G.; Grabis, J.; Laschke, K.; Boysen, H.; Schneider, J.; Frey, F. *J. Mater. Sci.* **1995**, *30*, 1621−1625.

Table 1. Samples Studied by EXAFS and Δk ($Å^{-1}$) Available for Analysis

sample	synthesis procedure[a]	W L_{III}-edge Δk ($Å^{-1}$)	Zr K-edge Δk ($Å^{-1}$)
(1) ZrO_2	commercial monoclinic	N/A	1.0−16.43
(2) ZrO_2	SG 600 °C, crystalline	N/A	1.0−16.46
(3) ZrO_2	SG 200 °C, 8% organic, amorphous	N/A	1.0−16.45
(4) ZrO_2	SG 110 °C, 35% organic, amorphous	N/A	1.0−16.0
(5) WO_3	commercial monoclinic	1.0−13.62	N/A
(6) WO_3	SG 600 °C, crystalline	1.0−15.56	N/A
(7) WO_3	SG 350 °C, 4% organic, poorly crystalline	1.0−15.56	N/A
(8) WO_3	SG 110 °C, 12% organic, amorphous	1.0−15.56	N/A
(9) ZrW_2O_8	SG 1200 °C, crystalline cubic	1.0−16.00	2.0−16.25
(10) ZrW_2O_8	SG, 740 °C, crystalline trigonal	1.0−16.00	2.0−16.10
(11) ZrW_2O_8	SG 600 °C, 0% organic, amorphous	1.0−16.00	2.0−15.00
(12) ZrW_2O_8	SG 110 °C, 30% organic, amorphous	1.0−16.00	2.0−15.00

[a] SG = nonhydrolytic sol−gel; N/A = not applicable.

the fitting procedure using this model. An appropriate starting value of E_0 for the Zr−O shell was determined to be −14.94 eV by fitting to the data for a commercial monoclinic zirconia sample (sample 1).

The tungsten L_{III}-edge EXAFS data were compared with models derived from the crystal structures of monoclinic WO_3,[35] cubic ZrW_2O_8,[7] and trigonal $ZrMo_2O_8$.[12] As the local tungsten environment in monoclinic WO_3 is irregular (six distinct W−O distances in the range 1.73−2.19 Å for each tungsten) the W−O distances were not all varied during the fitting procedure using this model. In cubic ZrW_2O_8 there are two crystallographically distinct tungsten sites with each site having 3 + 1 oxygen coordination and three zirconiums in the second coordination shell. As the W−O bond lengths for the two tungsten sites are similar, the EXAFS data were modeled assuming that the oxygen coordination for each of the tungsten sites was the same.

Results

Crystallization Studies. Powder diffraction patterns showing the structural evolution of the ZrO_2, WO_3 and ZrW_2O_8 gels on heating are presented in Figure 1. The heat-treated ZrO_2 gels started to show some signs of crystallization at 300−400 °C and at 450 °C the powder pattern was consistent with the presence of some very poorly crystalline tetragonal (PDF # 42-1164) or cubic zirconia (PDF # 27-997). At 600 °C a mixture of cubic/tetragonal and a small amount of monoclinic ZrO_2 (PDF # 37-1484) had formed. Even the raw WO_3 gel shows evidence for the presence of crystalline WO_3 and at 400 °C there was undoubtedly monoclinic WO_3 (PDF # 43-1035) present in the sample. The ZrW_2O_8 heat-treated gels showed no evidence for any crystallization below 600 °C. Crystallization occurred at about 740 °C to a phase that was identified as being structurally related to trigonal $ZrMo_2O_8$ by comparison of the observed powder diffraction pattern to that calculated for ZrW_2O_8 adopting the trigonal $ZrMo_2O_8$ structure (see Figure 2a).[12] As there are several materials with structures closely related to that of trigonal $ZrMo_2O_8$ ($P\bar{3}1c$, a = 10.14, c = 11.71 Å), for example the family

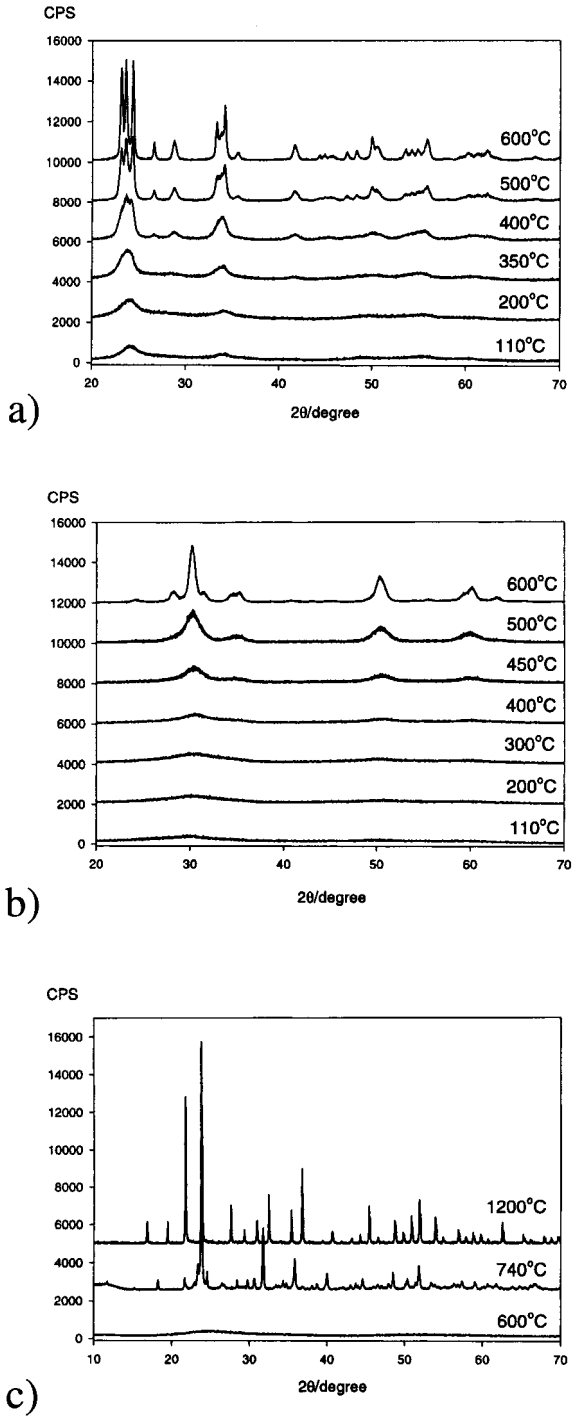

Figure 1. The crystallization of (a) WO_3, (b) ZrO_2, and (c) ZrW_2O_8 gels on heating. The ZrW_2O_8 gel crystallizes at a higher temperature than either the ZrO_2 or WO_3 gel.

MRe_2O_8 (M = Mn, Co, Ni, Zn) ($P\bar{3}$, a = 5.67−5.86 Å, c = 6.07−6.17 Å),[36] a comparison of the powder diffraction pattern calculated assuming that the new ZrW_2O_8 polymorph adopts the later structure was also performed (see Figure 2b). There is excellent agreement between the calculated patterns and all of the strong peaks in the observed data for both structural models. Trigonal $ZrMo_2O_8$ is reported to have lattice constants, a = 10.14 and c = 11.71 Å, that are comparable to those of our "trigonal" ZrW_2O_8, a = 9.81 and c = 11.73 Å

(35) Woodward, P. M.; Sleight, A. W.; Vogt, T. *J. Phys. Chem. Solids* **1995**, *56*, 1305−1315.

(36) Butz, A.; Miehe, G.; Paulus, H.; Strauss, P.; Fuess, H. *J. Solid State Chem.* **1998**, *138*, 232−237.

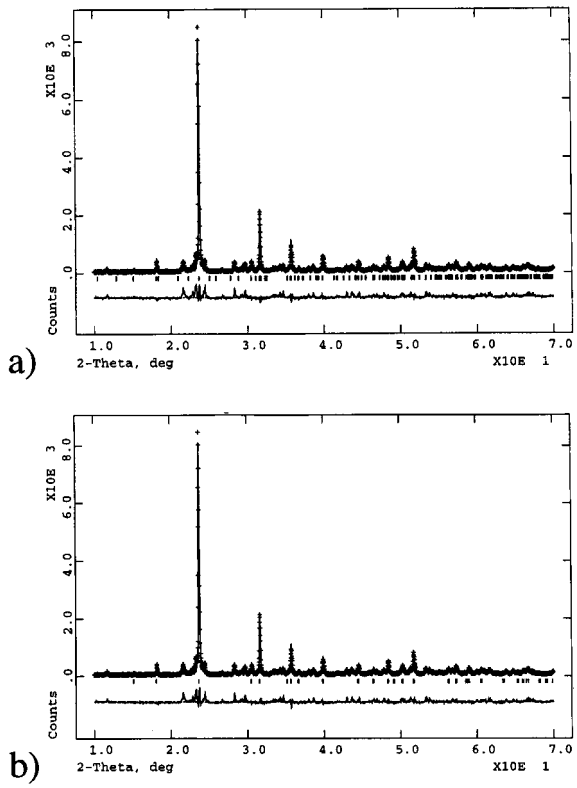

Figure 2. A comparison between the experimental powder pattern for trigonal ZrW_2O_8 and (a) the calculated powder pattern obtained by substituting W for Mo in the literature structure of trigonal $ZrMo_2O_8$ and (b) the calculated powder pattern obtained by substituting W for Re and Zr for Mn in the literature structure for $MnRe_2O_8$. In each case, the crosses are the experimental data, the solid line is the calculated pattern, tick marks indicate the calculated reflection positions, and a difference curve is plotted below the experimental and calculated patterns. The lattice constants and peak shape were varied to obtain the best match to the experimental data. For the $MnRe_2O_8$ model the atomic positions were also optimized.

assuming a $ZrMo_2O_8$-type structure (163 Å^3 per formula unit, calculated density 5.98 g cm^{-3}). If a $MnRe_2O_8$ structure is assumed, the diffraction data indexes well on a unit cell $a = 5.66$ and $c = 5.87$ Å (163 Å^3 per formula unit, calculated density 5.98 g cm^{-3}). The two unit cells are related by the transformation matrix (2,1,0;−1,1,0;0,0,2). An EDX examination of the new phase confirmed that it had a Zr:W ratio of ∼1:2. A pyconometric density determination for the trigonal ZrW_2O_8 sample gave a value of 6.33 ± 0.12 g cm^{-3} (the quoted precision estimate is one standard deviation based on four measurements) which is close to that expected for ZrW_2O_8 with a trigonal $ZrMo_2O_8$ structure (5.98 g cm^{-3}). Inspection of the powder pattern shown in Figure 1 for trigonal ZrW_2O_8 suggests that the sample also contains small amounts of monoclinic WO_3 (density 7.16 g cm^{-3}). However, there are additional weak peaks in this diffraction data that do not belong to any of the likely known impurity phases in this system (WO_3, ZrO_2, cubic ZrW_2O_8 (PDF # 13-557)). Many of these additional peaks can be indexed on a supercell of the trigonal $ZrMo_2O_8$ structure related to the subcell by elongation of the *c*-axis, $\mathbf{c}' = 1.5\mathbf{c}$. Treatment of ZrW_2O_8 gels in the temperature range where cubic ZrW_2O_8 is a thermodynamically stable phase typically led to the cubic phase plus, in some cases, small amounts of WO_3.

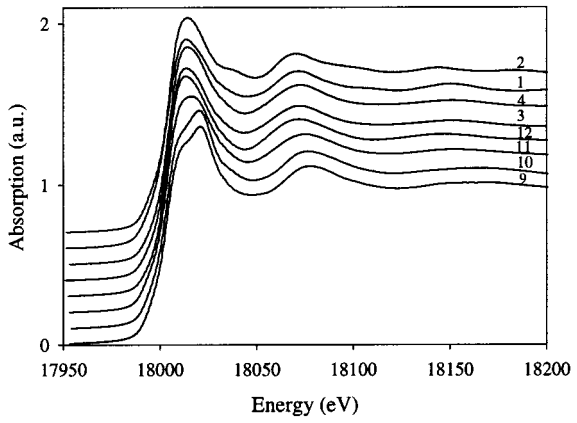

Figure 3. A comparison of the Zr K-edge XANES data for all the zirconium containing samples. The sample naming scheme is given in Table 1.

Several variations of the nonhydrolytic sol−gel preparation procedure were tried in an effort to produce cubic ZrW_2O_8 at low temperature. In some cases the cubic phase was found to crystallize along with the trigonal material. However, so far we have been unable to prepare samples containing more than ∼50% of the cubic phase.

EXAFS Studies. Zirconium K-Edge Data. The near-edge absorption spectra, raw EXAFS, and Fourier transform magnitudes for all the zirconium-containing samples are compared in Figures 3 and 4a,b, respectively. Figure 3 shows that the XANES for samples 9 and 10 (trigonal and cubic ZrW_2O_8) are very similar to one another and distinct from those of all the other samples. An inspection of Figure 4 indicates that the local structure in the as-prepared ZrO_2 (sample 4) and heat-treated ZrO_2 (sample 3) gels is very similar. The Fourier transform magnitudes for both materials show clear evidence for the presence of zirconium in the second coordination shell of the absorbing atom at a distance similar to that observed for monoclinic zirconia (sample 1). The local structures in samples 4 and 3 differ from that of the ZrO_2 gel heat-treated at 600 °C (sample 2) and the commercial monoclinic zirconia (sample 1) primarily in the second coordination shell. A comparison of the raw EXAFS for sample 2 with those in the literature for stabilized cubic and tetragonal zirconia[37] suggests that it is primarily tetragonal, rather than cubic, zirconia. The local structures for zirconium in the raw ZrW_2O_8 gel (sample 12) and the material heat-treated to 600 °C (sample 11) are similar. However, the fitting results (Table 2) indicate some subtle differences. The main difference between the local structure in these samples and that found in cubic ZrW_2O_8 and trigonal ZrW_2O_8 is the lack of any well-defined features in the second coordination shell corresponding to metal−metal distances. Cubic zirconium tungstate (sample 9) and trigonal zirconium tungstate (sample 10) have very similar zirconium environments, including the second coordination shell, as evidenced by the similarity of the FT magnitudes and the raw EXAFS. The results from fitting the Fourier filtered first shell data for samples 3, 4, 9, 10, 11, and 12 to the cubic ZrW_2O_8 model are shown in Table 2. The best fits are shown in Figure 5.

(37) Li, P.; Chen, I.-W.; Penner-Hahn, J. E. *Phys. Rev. B* **1993**, *48*, 10063−10073.

Table 2. First Shell Fitting Results for the Zr K-Edge EXAFS Data Assuming a Cubic ZrW_2O_8-Like Environment for Zirconium[a]

sample		R (Å)	σ^2 (Å^2)	N	average R (Å)
(3) ZrO_2, 200 °C, amorphous	Zr−O1	2.08	0.0029	3	2.14
	Zr−O2	2.20	0.0039	3	
(4) ZrO_2, 110 °C, amorphous	Zr−O1	2.08	0.0031	3	2.14
	Zr−O2	2.20	0.0042	3	
(9) ZrW_2O_8, cubic	Zr−O1	2.04	0.0027	3	2.08
	Zr−O2	2.11	0.0040	3	
(10) ZrW_2O_8, trigonal	Zr−O1	2.03	0.0012	3	2.08
	Zr−O2	2.13	0.0011	3	
(11) ZrW_2O_8, 600 °C, amorphous	Zr−O1	2.06	0.0036	3	2.12
	Zr−O2	2.17	0.0036	3	
(12) ZrW_2O_8, 110 °C, amorphous	Zr−O1	2.09	0.0027	3	2.15
	Zr−O2	2.20	0.0028	3	

[a] Fourier filtered data in the range 3−15 Å^{-1} were used in the analysis except for sample 12 where reasonable data were only available in the range 3−14 Å^{-1}. In each case E_0 was −15.2 eV.

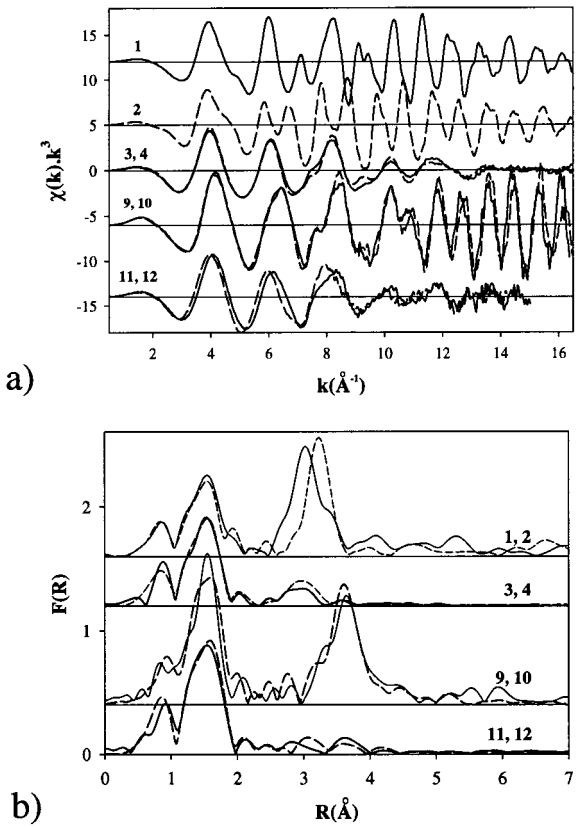

Figure 4. A comparison of (a) the raw Zr K-edge EXAFS data and (b) the FT magnitudes derived from these data for all the zirconium-containing samples. In the cases where two curves have been overplotted the solid line corresponds to the sample with the lower identification number.

It is notable that the average Zr−O bond lengths for samples 9 and 10 are considerably shorter than those for samples 3, 4, and 12, and that the average Zr−O bond length in sample 11 is intermediate between those observed for samples 9/10 and 3/4/12.

EXAFS Studies. Tungsten L_{III}-Edge Data. The near-edge absorption spectra, raw EXAFS, and Fourier transform magnitudes for all the tungsten-containing samples are compared in Figures 6 and 7a,b, respectively. The XANES data for sample 9 (cubic ZrW_2O_8) show a feature (indicated by an arrow in Figure 6)

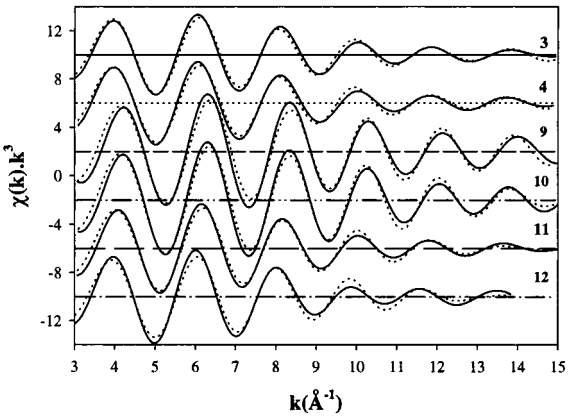

Figure 5. The best fit of a 3 + 3 coordination model for zirconium to the Fourier filtered first shell EXAFS data for samples 3, 4, 9, 10, 11, and 12. The solid lines are the Fourier filtered data and the dotted lines are the calculated best fits.

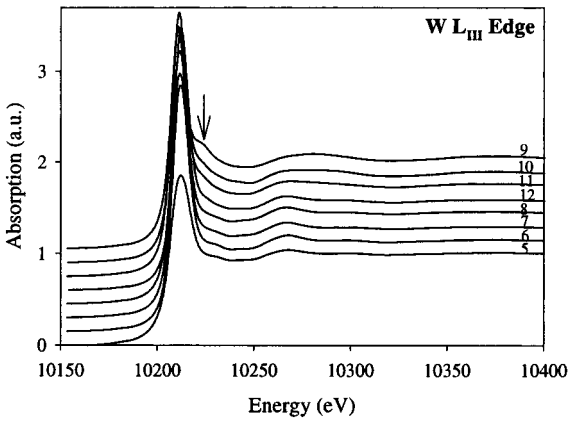

Figure 6. A comparison of the W L_{III}-edge XANES data for all the tungsten containing samples. The sample naming scheme is given in Table 1.

immediately after the white line that is not present for samples 5, 6, 7, and 8, and appears to be absent for sample 12. An inspection of the data presented in Figure 7 indicates that samples 9 (cubic ZrW_2O_8) and 10 (trigonal ZrW_2O_8) have a similar local structure around tungsten. Additionally, the as-made and 350 °C heat-treated WO_3 gels have similar local structures. However, the as-made and 600 °C heat-treated ZrW_2O_8 gels (samples 12 and 11, respectively) are significantly different. Both of these samples show a weak feature, just above the noise level, in the FT magnitude at a distance that is reasonable for a metal in the second coordination shell of the tungsten, but the first coordination shell for the two materials is different. The results from fitting the Fourier filtered first shell (W−O) data for samples 6, 7, 8, 9, 10, 11, and 12 to a 3 + 1 coordination model are shown in Table 3 and the fits are shown in Figure 8. With the exception of samples 9, 10, and perhaps 6, these fits are of poor quality, indicating that the model used is not appropriate for most of the samples. It should be noted that the refined parameters for sample 6 are very different from those obtained for the other samples, indicating that the 3 + 1 tetrahedral starting model, based on the coordination environment found in cubic ZrW_2O_8, is not appropriate for sample 6. A reasonable fit to the data could be obtained for samples 6, 7, 8, and 12 using an irregular six-coordinate model based on the structure of mono-

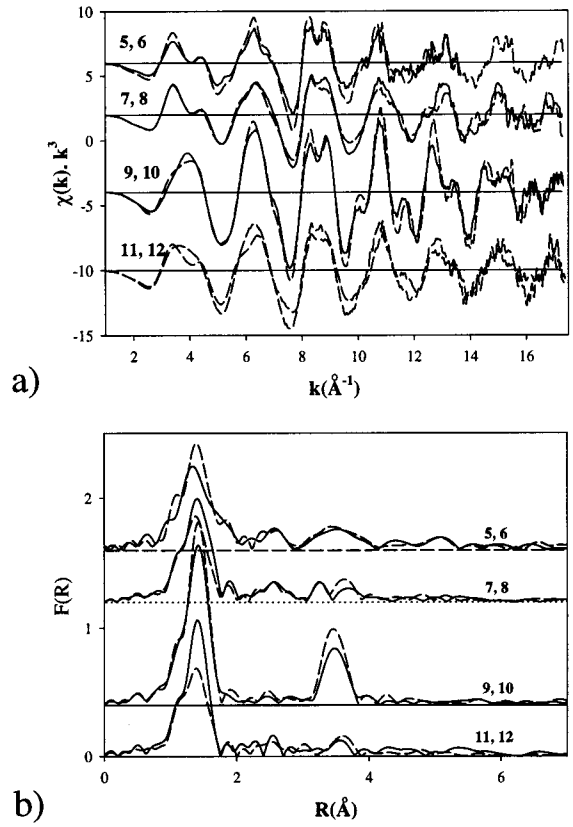

Figure 7. A comparison of (a) the raw W L_{III}-edge EXAFS data and (b) the FT magnitudes derived from these data for all the tungsten-containing samples. In the cases where two curves have been overplotted the solid line corresponds to the sample with the lower identification number.

Table 3. First Shell Fitting Results for the W L_{III}-edge EXAFS Data Assuming a Cubic ZrW_2O_8-Like Environment[a]

sample		*R* (Å)	σ^2 (Å^2)	*N*
(6) WO_3, 600 °C, monoclinic	W−O1	2.13	0.0040	1
	W−O2	1.79	0.0040	3
(7) WO_3, 350 °C	W−O1	1.75	0.0051	1
	W−O2	1.79	0.0051	3
(8) WO_3, 110 °C, amorphous	W−O1	1.76	0.0074	1
	W−O2	1.80	0.0074	3
(9) ZrW_2O_8, cubic	W−O1	1.72	0.0019	1
	W−O2	1.80	0.0019	3
(10) ZrW_2O_8, trigonal	W−O1	1.73	0.0015	1
	W−O2	1.80	0.0015	3
(11) ZrW_2O_8, 600 °C, amorphous	W−O1	1.75	0.0037	1
	W−O2	1.80	0.0037	3
(12) ZrW_2O_8, 110 °C, amorphous	W−O1	1.75	0.0066	1
	W−O2	1.79	0.0066	3

[a] Data in the range 2.5−15.5 Å^{-1} were used in every case. The thermal parameters for the two oxygen shells were constrained to be the same. E_0 for all the analyses was fixed at −8.765 eV.

clinic WO_3 (see Figure 9). The first shell Fourier filtered EXAFS data for samples 6, 9, 11, and 12 are compared in Figure 10. While the data for samples 6 and 12 are similar to one another, the data for the heat-treated amorphous ZrW_2O_8 gel (sample 11) is a better match to that for the tetrahedral tungsten environment found in cubic ZrW_2O_8 (sample 9) than to that for samples 6 or 12.

Discussion

The crystallization behavior of our ZrO_2 and WO_3 samples was in good agreement with previous reports

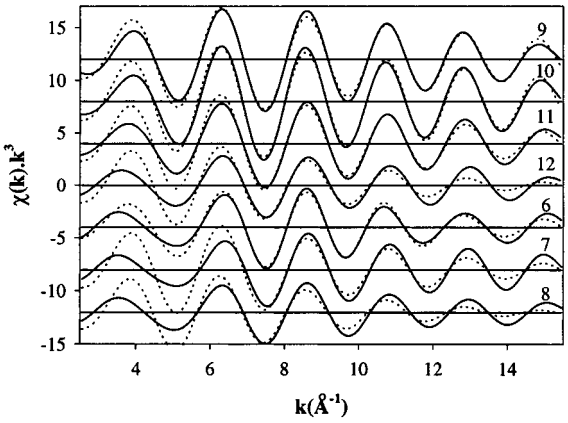

Figure 8. The best fit of a 3 + 1 coordination model for tungsten to the Fourier filtered first shell EXAFS data for samples 6, 7, 8, 9, 10, 11, and 12. The solid lines are the Fourier filtered data and the dotted lines are the best fits. The best fit parameters are given in Table 3.

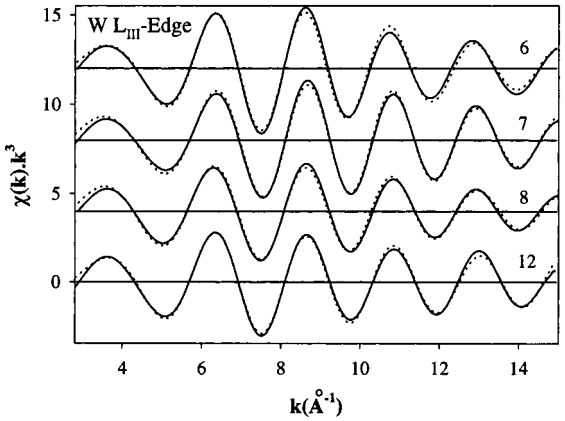

Figure 9. The Fourier filtered first shell W L_{III}-edge EXAFS data for samples 6, 7, 8, and 12 are in good agreement with an irregular coordination environment like that found in monoclinic WO_3. The solid lines are the data and the dashed lines were calculated from a monoclinic WO_3-like model.

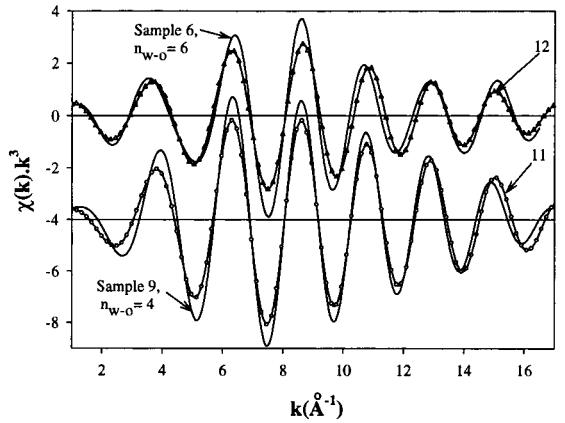

Figure 10. A comparison of the W L_{III}-edge Fourier filtered first shell EXAFS data for samples 6, 9, 11, and 12. The data for sample 11 appears to be intermediate between those for samples 6/12 and sample 9.

of the nonhydrolytic sol−gel preparation of these compounds.[23] However, the crystallization of a new metastable ZrW_2O_8 polymorph was a complete surprise to us. While we have not yet been able to obtain a detailed structure analysis for our new ZrW_2O_8 polymorph, we believe that (i) the EDX determination of the materials'

composition, (ii) the conversion of the new material to cubic ZrW_2O_8 at high temperature, (iii) the close match between the strong peaks in the observed powder diffraction pattern and those calculated assuming a trigonal $ZrMo_2O_8$ model with tungsten substituted for molybdenum or a $MnRe_2O_8$ structural model with zirconium in place of manganese and tungsten in place of rhenium, (iv) the striking similarity between the EXAFS data for cubic ZrW_2O_8 and that for the new polymorph of ZrW_2O_8, and (v) the reasonable agreement between the measured density of our new ZrW_2O_8 polymorph and that expected for a trigonal $ZrMo_2O_8$- or $MnRe_2O_8$-type structure provide conclusive evidence that our new material is a close structural relative of both trigonal $ZrMo_2O_8$ and the MRe_2O_8 (M = Mn, Co, Ni, Zn) family of materials.

The MRe_2O_8 structure has the same layer connectivity as that found in $ZrMo_2O_8$, but the layers are distorted in a different way, leading to a smaller unit cell.[36] The two cells are related by the transformation matrix (2,1,0;−1,1,0;0,0,2). In trigonal $ZrMo_2O_8$ there is a two-layer repeat sequence along the *c*-axis, but in the MRe_2O_8 structures there is a one-layer repeat sequence. The observation that many of the additional weak peaks in our trigonal ZrW_2O_8 pattern can be indexed on a unit cell with the *c*-axis one and a half times longer than that of trigonal $ZrMo_2O_8$ may indicate the occurrence of a three-layer repeat pattern in trigonal ZrW_2O_8.

The very close agreement between the EXAFS spectra for cubic ZrW_2O_8 and a tungstate with a trigonal $ZrMo_2O_8$-type structure is to be expected as EXAFS is only sensitive to the local structure of the material and, on the basis of their crystal structures, the local environment of the metals (nearest neighbor and next-nearest neighbor atoms) in these two different structure types is almost identical. However, there are some slight differences in the local structure for the two materials. In trigonal $ZrMo_2O_8$ the zirconium has six equal Zr−O distances rather than the 3 + 3 coordination found in cubic ZrW_2O_8. This difference appears to be present in our trigonal and cubic ZrW_2O_8 samples. While we obtained good fits to the Fourier filtered first shell data for both samples 9 and 10 (cubic and trigonal ZrW_2O_8) using a 3 + 3 coordination model derived from the crystal structure of cubic ZrW_2O_8, our attempts to model the data using six equal Zr−O distances led to a good fit for the trigonal ZrW_2O_8 data but a poor fit at high *k* for the cubic ZrW_2O_8 data.

The production of a trigonal polymorph of ZrW_2O_8 by low-temperature methods is at first sight hard to understand. Our previous work on the low-temperature preparation (∼650 °C) of ZrW_2O_8, and literature reports on the preparation of HfW_2O_8[38] and ZrW_2O_8[39] by the dehydration of precursors of the type $MW_2O_7(OH/Cl)_2 \cdot 2H_2O$ (M = Zr, Hf), have only produced cubic MW_2O_8. However, in the case of $ZrMo_2O_8$, where we recently prepared a new cubic polymorph via a dehydration route of this type,[16] the cubic material is much less dense than the trigonal material and the cubic form is metastable with respect to the trigonal form under the conditions used for its preparation. Our new trigonal ZrW_2O_8 (∼163 Å^3/formula unit, calculated density 5.98 g cm^{-3} at room temperature) is denser than the well-known ambient pressure phase cubic ZrW_2O_8 (∼192 Å^3/formula unit, 5.08 g cm^{-3} at room temperature) and the recently reported high-pressure phase γ-ZrW_2O_8 (∼182 Å^3/formula unit, 5.36 g cm^{-3} at room temperature).[6] These density differences combined with the observations that (i) the new trigonal phase does not convert to the cubic phase on prolonged heating at low temperature (it decomposes to the binary oxides after heating for ∼2 days at 700 °C) and (ii) the cubic phase is thermodynamically unstable with respect to the binary oxides below 1105 °C are consistent with the idea that trigonal ZrW_2O_8 is thermodynamically more stable than cubic ZrW_2O_8 at low temperatures (as we found for the molybdate). If this is true, then there must be a significant kinetic barrier preventing the conversion of cubic ZrW_2O_8 to trigonal ZrW_2O_8 at atmospheric pressure and moderate temperatures. This line of reasoning suggests that it might be possible to convert cubic ZrW_2O_8 to the trigonal form by the application of pressure and heating to overcome any kinetic barrier to the conversion. To date, studies of cubic ZrW_2O_8 under pressure (up to 8 GPa) have only been performed at ambient temperature. These experiments found a low-pressure cubic-to-orthorhombic phase transition[6] and a higher pressure amorphization.[8]

The EXAFS data indicate that on heating the as-made ZrW_2O_8 gel the local environments for the metals move toward those seen in the final product prior to crystallization. For example, our fits (Table 2) of the first shell zirconium EXAFS data to a 3 + 3 coordination model (as found in cubic ZrW_2O_8) for the raw gel (sample 12), the 600 °C heat-treated amorphous ZrW_2O_8 gel (sample 11), and the crystalline trigonal ZrW_2O_8 (sample 9) gave average Zr−O bond lengths of 2.15, 2.12, and 2.08 Å, respectively. A decrease in the apparent value for the refined bond lengths is unreasonable if the zirconium atom in each sample is really coordinated to only six oxygen atoms, as it would imply an increase in valence for the central zirconium atom.[40−42] However, it is entirely consistent with a reduction in coordination number for zirconium as the gel is heated. The zirconium in the amorphous raw gel presumably has an average coordination number greater than six and this average approaches six as the sample is heat-treated. A reduction in average Zr−O bond length is associated with the reduction in coordination number so that the bond valence sum rule for the zirconium is satisfied.[40−42]

The tungsten coordination environment found in many crystalline and amorphous oxides is irregular. Although our W L_{III}-edge EXAFS data were compared to a model based on the monoclinic WO_3 structure with six distinct W−O distances, it was not possible to perform a meaningful complete numerical analysis using such a model because of the large number of correlated parameters. A complete analysis using a 3 + 1 coordination model was performed so that the

(38) Palitsyna, S. S.; Mokhosoev, M. V.; Krivobok, V. I. *Bull. Acad. Sci. USSR, Div. Chem. Sci.* **1977**, 611−613.
(39) Closmann, C.; Sleight, A. W. *J. Solid State Chem.* **1998**, *139*, 424−426.
(40) Brown, I. D.; Wu, K. K. *Acta Crystallogr.* **1976**, *B32*, 1957−1959.
(41) Brown, I. D. *Structure and Bonding in Crystals*; Academic Press: 1981; Vol. II, Chapter 14, pp 1−30.
(42) Brown, I. D.; Altermatt, D. *Acta Crystallogr.* **1985**, *B41*, 244−247.

quality of the fit to this model could be used as a guide to the tetrahedral tungsten content of the sample.

No trend in the bond lengths obtained by fitting the tungsten EXAFS data to the 3 + 1 model can be seen (Table 3). However, a trend in the refined thermal parameters is apparent and the XANES (Figure 6) show some features of interest. The 3 + 1 model only gave a reasonable fit for samples 9 and 10 (cubic and trigonal ZrW_2O_8), suggesting that even in the 600 °C heat-treated ZrW_2O_8 gel (sample 11) the tungsten is not predominantly four-coordinated. However, the first shell Fourier filtered data for sample 11 seems to be intermediate between those observed for the cubic and trigonal ZrW_2O_8 and the materials treated at lower temperatures or monoclinic WO_3 (see Figure 10). We interpret the latter observation as indicating that the 600 °C heat-treated ZrW_2O_8 sample contains some four-coordinate tungsten along with some higher coordination number environments. Both the thermal parameters obtained from fitting using the 3 + 1 model and the XANES data seem to support the idea that the 600 °C heat-treated ZrW_2O_8 sample contains more tetrahedral tungsten than the as-prepared gel, but less than that found in fully crystallized ZrW_2O_8. The thermal parameters for the tungsten in the 600 °C heat-treated ZrW_2O_8 sample are intermediate between those for the WO_3 and ZrW_2O_8 raw gels and those found for crystalline ZrW_2O_8. This decrease in the thermal parameters after heat treatment implies that the distribution of bond lengths more closely approximates the 3 + 1 coordination model after heating. Typically, XANES studies that are designed to examine the relative amounts of tetrahedral and octahedral tungsten in a sample make use of the pre-edge features found in W L_I-edge spectra.[43−47] While these sensitive pre-edge features do not occur in L_{III} edge spectra, there are literature reports of XANES features associated with the presence of tetrahedrally coordinated tungsten in a sample.[46] Compounds such as $CaWO_4$,[44,46] Na_2WO_4,[44] and $FeWO_4Cl$[48] that contain tetrahedrally coordinated tungsten display a peak in their L_{III} edge spectra at slightly higher energies than those of the white line. Our W L_{III} edge spectrum for cubic ZrW_2O_8 clearly shows such a peak (marked with an arrow in Figure 6) and the spectra for samples 10 (trigonal ZrW_2O_8) and 11 (600 °C ZrW_2O_8) show a shoulder on the white line at roughly the same energy as this peak. There is no evidence of a shoulder in this region for the other samples.

Acknowledgment. This research was supported by the National Science Foundation through Grant DMR-9623890. C.L. is grateful to the Georgia Rotary Student Program for a scholarship and to the German National Merit Foundation for travel support. We are indebted to Dr. Ingrid Pickering for assistance with the EXAFS data collection. The EXAFS facilities at the Stanford Synchrotron Radiation Laboratory are operated as part of the SSRL Biotechnology Program which is supported by the National Institutes of Health, National Center for Research Resources, Biomedical Technology Program, and by the Department of Energy, Office of Biological and Environmental Research.

CM9805065

(43) Horsley, J. A.; Wachs, I. E.; Brown, J. M.; Via, G. H.; Hardcastle, F. D. *J. Phys. Chem.* **1987**, *91*, 4014−4020.
(44) Hilbrig, F.; Gobel, H. E.; Knozinger, H.; Schmelz, H.; Lengeler, B. *J. Phys. Chem.* **1991**, *95*, 6973−6978.
(45) Kuzmin, A.; Purans, J. *J. Phys. IV* **1997**, *7*, C2-971−C2-973.
(46) Balerna, A.; Bernieri, E.; Burattini, E. *Nucl. Inst. Methods Phys. Res.* **1991**, *A308*, 240−242.
(47) Purans, J.; Kuzmin, A.; Parent, P.; Dexpert, H. *Physica B* **1995**, *208* and *209*, 307−308.
(48) Cho, J.-H.; Yoon, J.-B.; Park, N.-G.; Kim, Y.-I.; Han, K.-S. *Jpn. J. Appl. Phys.* **1997**, *36*, 5605−5609.